Hydrogel-Coated Dental Device with Adhesion-Inhibiting and Colony-Suppressing Properties

Liying Peng,[∥] Li Chang,[∥] Mengting Si, Jiuxiang Lin, Yan Wei,* Shutao Wang, Hongliang Liu,* Bing Han,* and Lei Jiang

Cite This: *ACS Appl. Mater. Interfaces* 2020, 12, 9718−9725
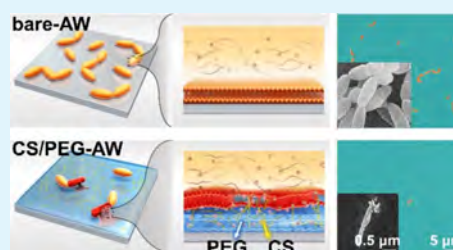
Read Online

ACCESS | Metrics & More | Article Recommendations | Supporting Information

ABSTRACT: Bacterial infection is the main cause of implantation failure worldwide, and the importance of antibiotics on medical devices has been undermined because of antibiotic resistance. Antimicrobial hydrogels have emerged as a promising approach to combat infections associated with medical devices and wound healing. However, hydrogel coatings that simultaneously possess both antifouling and antimicrobial attributes are scarce. Herein, we report an antimicrobial hydrogel that incorporates adhesion-inhibiting polyethylene glycol (PEG) and colony-suppressing chitosan (CS) as a dressing to combat bacterial infections. These two polymers have important environmentally benign characteristics including low toxicity, low volatility, and biocompatibility. Although hydrogels containing PEG and CS have been reported for applications in the fields of wound dressing, tissue repair, water purification, drug delivery, and scaffolds for bone regeneration, there still has been no report on the application of CS/PEG hydrogel coatings in dental applications. Herein, this biointerface shows superior activity in early-stage adhesion inhibition (98.8%, 5 h) and displays remarkably long-lasting colony-suppression activity (93.3%, 7 d). Thus, this novel nanomaterial, which has potential as a dual-functional platform with integrated antifouling and antimicrobial functions with excellent biocompatibility, might be used as a safe and effective antimicrobial coating in biomedical device applications.

KEYWORDS: *adhesion-inhibiting, antibacterial, polyethylene glycol, chitosan, hydrogel*

1. INTRODUCTION

In modern medicine, implant appliances have been widely employed to repair defects, fix the physiological dysfunction, and rectify malalignment.[1] However, the pathogenicity caused by abnormal bacterial adhesion and colonization on these appliances poses a severe threat to the host flora ecosystems and organ functions.[2,3] Designing antimicrobial medical apparatuses remains a challenge worldwide. Although the local or systemic administration of various antimicrobial medications decreases bacterial infection, the transient effect and adverse drug reactions limit their use.[4] Environmental concerns and economic demands highlight the urgent need for functional materials that can efficiently elicit antimicrobial activity.[5,6] Because of their high water content and resemblance to biological soft tissues, hydrogels can easily integrate into the biological environment of the human body, and antimicrobial hydrogels have emerged as an important platform to combat infections associated with medical devices and wound healing. However, the reports of hydrogels as antimicrobial coatings that simultaneously fulfill the requirements of anti-adhesive and antimicrobial attributes and biocompatibility are scarce. Therefore, in this study, we aimed to create antifouling antimicrobial hydrogels, which can be easily applied to medical implants such as stainless steel as a coating to prevent infections. To achieve this goal, we choose polyethylene glycol (PEG), a recognized environ-

mentally friendly polymer, as the functional component for adhesion resistance of the coating. Modifying surfaces with PEG—known as PEGylation—has been the benchmark for achieving highly resistant antifouling surfaces that prevent protein adsorption.[7−9] Our group has recently demonstrated that PEGylated dental materials exhibit excellent antibacterial properties because of their ability to form a stable thin water layer through hydrogen bonding interactions with their many ether groups.[10] Meanwhile, to enhance the antimicrobial potency of the film, chitosan (CS) was chosen as the antimicrobial component. CS, which is produced commercially by the deacetylation of chitin and exhibits good nontoxicity, biocompatibility, and biodegradability, has been widely used to efficiently suppress colony formation.[11,12] The antibacterial activity of CS is attributed to its positively charged quaternary ammonium moieties, which exert strong electrostatic interactions with the negatively charged bacterial cell surface, leading to microbial membrane disruption and microbe death and thus preventing subsequent biofilm formation.[13] Although hydrogels containing PEG and CS, which are mostly based on

PEGylated CS in the form of grafting copolymers, have been reported for applications in some fields, such as wound dressing and drug delivery, there has still been no report for the application of CS/PEG hydrogel coatings in the surface modification of medical equipment, especially dental devices.[14−21] Considering practical applications, functional hydrogel-coated materials combining the stable adhesion-inhibiting properties of PEG and colony-suppressing activities of CS may offer great potential and several advantages to combat infections in a more biocompatible and environmentally friendly way.

Herein, we report facile synthesis of a CS/PEG hydrogel-coated dental appliance (i.e., a stainless-steel archwire, AW) with optimized hydrophilicity and surface potential, simultaneously achieving anti-adhesion and antibacterial properties (Figure 1). The cross-linked PEG network can effectively
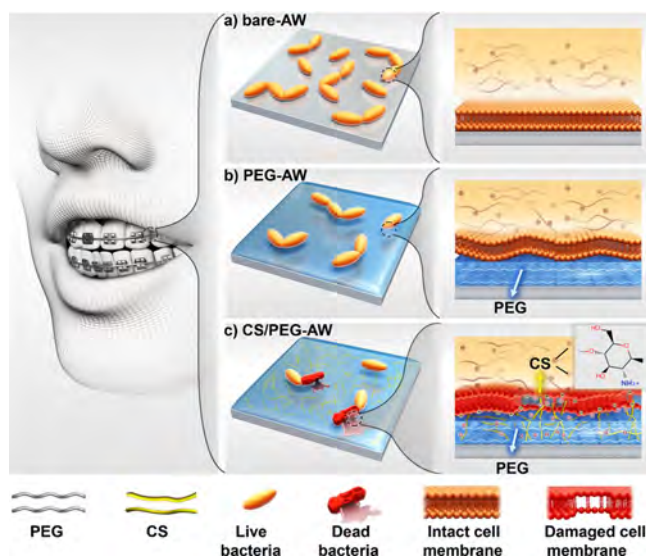

Figure 1. Schematic illustration of the design of a dental appliance with both adhesion-inhibiting and antibacterial capabilities. (a) Significant aggregation of bacteria on bare stainless-steel AW. (b) PEGylation of stainless-steel AW can significantly reduce bacterial adhesion owing to the existence of a thin water layer caused by PEG. (c) Stainless-steel AW with CS/PEG hydrogel coating exhibits both adhesion-inhibiting and antibacterial capabilities.

absorb water through hydrogen bonds to form a thin water layer, endowing the CS/PEG-AW with anti-adhesion properties. Meanwhile, the interpenetrating CS chains with positively charged quaternary ammonium salts can rupture the negatively charged bacterial cell membrane via electrostatic interactions and thus efficiently suppress the adhesion of bacterial colonies (Figure 1c). In comparison, bacteria obviously adhered to bare-AW (Figure 1a). Moreover, PEGylation of AW (PEG-AW) can only reduce bacterial adhesion (Figure 1b) without killing the adhered bacteria.

2. RESULTS AND DISCUSSION

We introduced the CS/PEG hydrogel coating onto AWs by combining silane chemistry and subsequent copolymerization. In the first step, we generated an alkene-terminated silanized AW. Next, free radical copolymerization was carried out by submerging the silanized AW in a reaction solution containing CS (poly(beta-(1,4)-D-glucosamine)) and mPEG-acrylate to form a CS/PEG primer, which was composed of a cross-linked

PEG network interpenetrated with CS chains (CS/PEG-AW, Figure S1). The successful synthesis of PEG- and CS/PEG-coated AWs was confirmed by comparing the surface composition of bare-AW, PEG-AW, and CS/PEG-AW using X-ray photoelectron spectroscopy (XPS) (Figure 2a−d). The
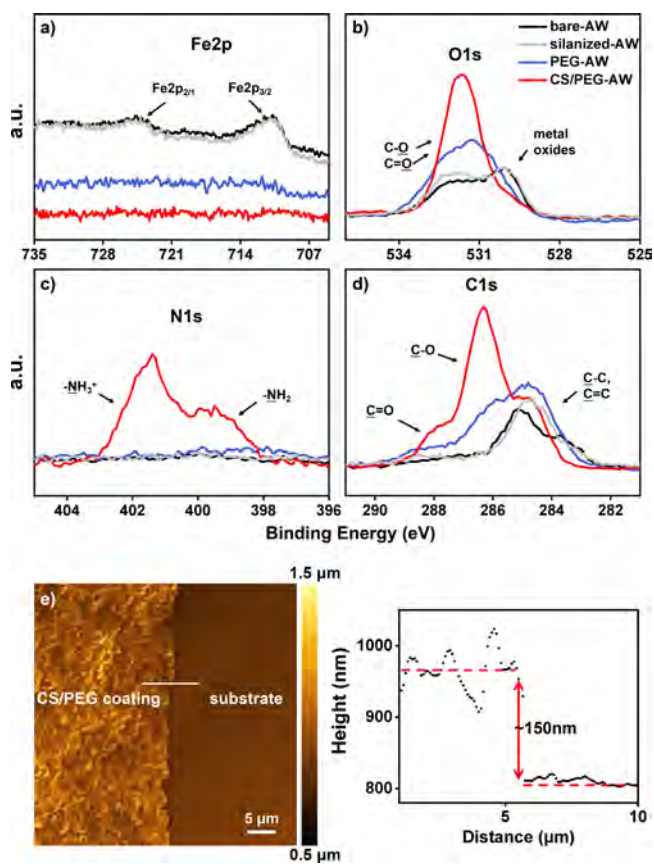

Figure 2. In XPS analysis, the existence of the PEG and CS/PEG coating on the stainless-steel AW was indicated by the attenuation of the Fe signal (a) and metal oxide signal (b) and the increased proportion of carbon atoms at approximately 286.4 eV (d). Presence of the nitrogen signal (c) on the stainless-steel alloy confirmed the existence of CS in the CS/PEG coating. (e) CLSM image of the CS/PEG hydrogel coating on a silicon wafer substrate. The height of the cross section of the CLSM image shows that the thickness of the CS/PEG coating is approximately 150 nm.

binding energies of Fe 2p (Figure 2a) obtained from the bare-AW and silanized-AW resolved into two peaks: a peak at 711.0 eV assigned to Fe $2p_{3/2}$ and another at 724.6 eV assigned to Fe $2p_{1/2}$.[22] The attenuation of the Fe signal in PEG-AW and CS/PEG-AW indicated the existence of a polymeric layer on the surfaces. In the O 1s core-level spectra (Figure 2b), there is a major peak at ∼530 eV corresponding to metal oxides on bare-AW and silanized-AW. This peak is less pronounced on PEG-AW and CS/PEG-AW, but on these materials, a significant peak corresponding to C═$\underline{O}$ and C−$\underline{O}$ species of PEG and CS units appears (∼532 eV).[23] The nitrogen content on bare-AW, silanized-AW, and PEG-AW is rather negligible as there is no nitrogen in them. In contrast, the N 1s core-level spectra (Figure 2c) of CS/PEG-AW can be decomposed into two components, an amine group (−$\underline{N}H_2$ at 399.4 eV) and an ammonium ion (−$\underline{N}H^{3+}$ at 401.6 eV); the latter is associated with the partial protonation of amino groups because CS is a weak polybase.[24] The C 1s spectra of the AW surface (Figure
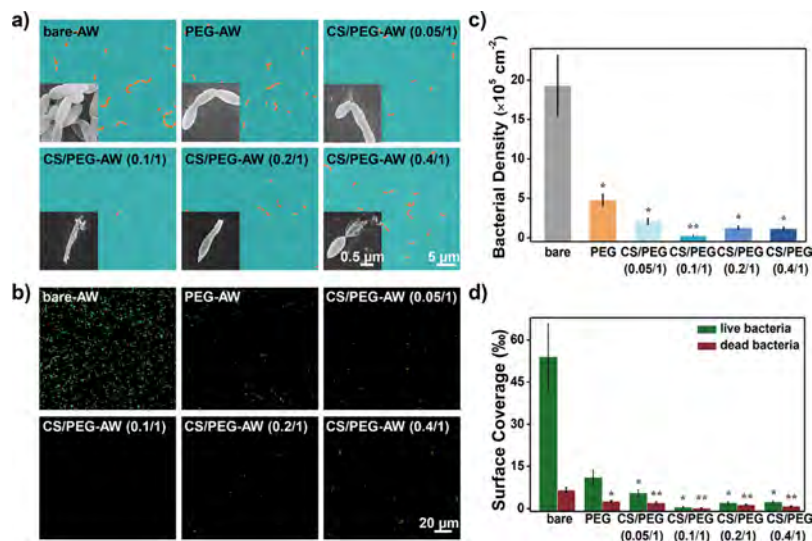
Figure 3. Antibacterial performance of bare-AW, PEG-AW, and CS/PEG-AW. (a) SEM images of bare-AW, PEG-AW, and CS/PEG-AW after incubation in bacterial suspensions for 5 h. (b) Fluorescence microscopy images of bare-AW, PEG-AW, and CS/PEG-AW after incubation in bacterial suspensions for 5 h. The live and dead bacteria stained green and red, respectively. (c) Quantitative evaluations of live bacterial adhesion on bare-AW, PEG-AW, and CS/PEG-AW according to the fluorescence microscopy images. Error bars represent the standard error based on 10 repeated measurements ($n = 10$). (d) Surface coverage of live and dead bacteria on bare-AW, PEG-AW, and CS/PEG-AW shown on the fluorescence microscopy images. Error bars represent the standard error based on 10 repeated measurements ($n = 10$). $*P < 0.05$; $**P < 0.01$ from data obtained in the bare-AW group.
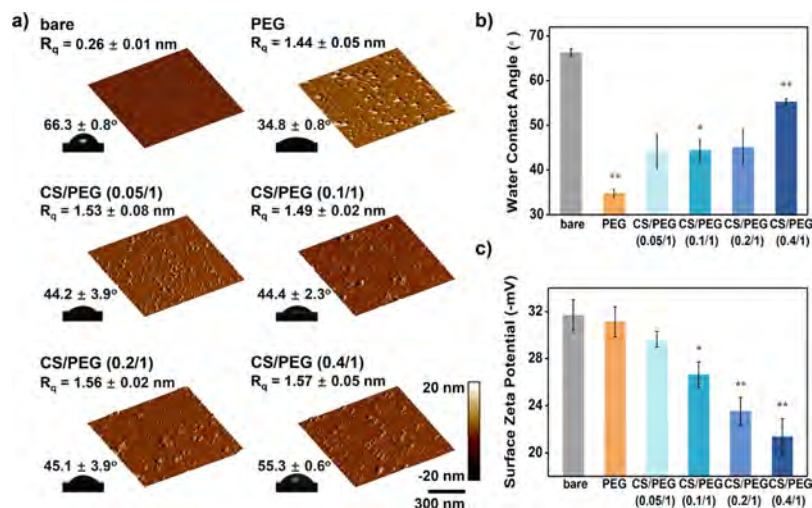

Figure 4. Unveiling the mechanism of antibacterial activity on bare, PEG, and CS/PEG samples. (a) Surface morphologies obtained from AFM. (b) WCA for bare and surface-coated stainless-steel sheets. (c) Surface zeta potential gradually decreased with the addition of the positively charged CS coating. Error bars represent the standard error based on three repeated measurements ($n = 3$). $*P < 0.05$; $**P < 0.01$ from data obtained in the bare group.

2d) can be deconvoluted into three peaks at 284.9, 286.4, and 288.5 eV, corresponding to $\underline{C}-C$ (or $\underline{C}=C$), $\underline{C}-O$, and $\underline{C}=O$ bonds, respectively. Compared with that on bare-AW, the number of carbon atoms in $\underline{C}-O$ (286.4 eV) bonds on PEGylated AW increases, while the proportion of carbon atoms in $\underline{C}-C$ bonds (284.9 eV) is reduced.[25,26] Meanwhile, the C 1s core-level spectra on CS/PEG-AW are in good agreement with the carbon atoms present in the CS molecule.[24] The full XPS spectra of bare-AW, silanized-AW, and CS/PEG-AW also confirmed the structure and the changes in the synthetic process (Figure S2a−c). These XPS results confirmed the successful coating of stainless-steel AWs with PEG and CS/PEG films. Confocal laser scanning

microscopy (CLSM) images indicated that the thickness of the CS/PEG-coating was approximately 150 nm (Figure 2e).

We chose *Streptococcus mutans* UA159 (*S. mutans* UA159),[27] a typical Gram-positive pathogenic strain, to evaluate the antibacterial activity of bare-AW, PEG-AW, and CS/PEG-AW. Scanning electron microscopy (SEM) images (Figure 3a) revealed a general trend of adhesive bacterial density and the fine structures of bacteria at high magnification. Significant adhesion and aggregation of *S. mutans* were observed on bare-AW. On PEG-AW, high bacterial adhesion inhibition was observed without disruption of the cell membrane, which is probably attributed to the adhesion-inhibiting property of cross-linked PEG. On the other hand, bacterial adhesion on CS/PEG-AW decreased more rapidly with different degrees of
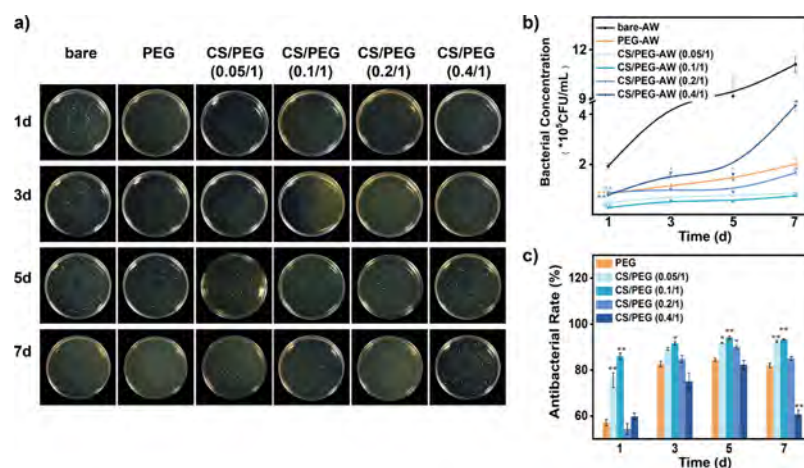
Figure 5. Long-term antibacterial performance of bare-AW, PEG-AW, and CS/PEG-AW. (a) Typical images of cultivated *S. mutans* colonies from the specimens after incubation. (b) Quantitative evaluations of bacterial colonies on the specimens. *$P < 0.05$; **$P < 0.01$ from data obtained in the bare-AW group. (c) Long-term antibacterial rates against *S. mutans*. *$P < 0.05$; **$P < 0.01$ from the antibacterial rate obtained in the PEG-AW samples. Error bars represent the standard error based on three repeated measurements ($n = 3$).

cell rupture and lysis, indicating that it has adhesion-inhibiting and colony-suppressing properties, which are most likely because of the synergistic effect between PEG and CS. We also used LIVE/DEAD cell viability assays to explore the antibacterial properties of the materials. Bacteria stained green are alive, while bacteria stained red are dead and have damaged membranes (Figure 3b). These results were in agreement with those from the SEM images. In addition, quantitative calculations of live bacterial density (Figure 3c) and the percentage area occupied by live/dead bacteria (Figure 3d) were evaluated using ImageJ software according to fluorescence microscopy images. A large surface of adherent bacteria (19.30×10^5 cm^{-2}) on bare-AW was alive, and the ratio of live/dead bacteria on the surface was high (8.18:1). The density of live bacteria on PEG-AW decreased to 4.78×10^5 cm^{-2}, whereas the live/dead bacterial ratio still remained at a relatively high level (4.29:1). We found that the antibacterial performance of CS/PEG-AW was strongly dependent on the CS/PEG mass ratio. For the CS/PEG-AW samples with a 0.1:1 CS/PEG optimal mass ratio, we found that the number of adhered bacteria was the lowest (0.24×10^5 cm^{-2}) and that most of the bacteria were dead. However, it should be noted that further increasing the CS concentration would lead to an increased number of both live and dead bacteria, which is in accordance with the SEM images. All the PEG-AW and CS/PEG-AW samples had significantly higher bacterial density than the bare-AW sample, especially the CS/PEG-AW (0.1:1) group. The statistical results of the live/dead bacterial surface coverage of each group were consistent with the bacterial density results. These findings demonstrate that the synergistic effect between PEG and CS endows the stainless-steel AW with excellent antibacterial properties, which is probably due to the combination of PEG's anti-adhesion properties and CS's antibacterial action.

To investigate why CS/PEG-AW (0.1:1) exhibits the best antibacterial performance, we explored the effects of surface morphology, surface wettability, and surface potential. In our case, the surface morphologies of different functional groups were characterized using atomic force microscopy (AFM). As shown in Figure 4a, bare-AW was relatively smooth with a surface roughness of approximately 0.26 nm. However, small nanoscale aggregates were observed for PEG-AW and CS/

PEG-AW with different CS/PEG mass ratios (0.05:1, 0.1:1, 0.2:1, and 0.4:1), which led to an increased surface roughness from 1.44 nm (PEG-AW) to 1.57 nm [CS/PEG-AW (0.4:1)], with no significant difference or regularity among these groups. Moreover, we compared the surface morphology of AWs with or without PEG and CS/PEG films under SEM. Figure S3 shows that all groups were made of stainless steel with irregular surface microstructures, showing no evident change after the coating of the AWs. Figure 4b shows the water contact angles (WCAs) of bare-AW, PEG-AW, and CS/PEG-AW with different CS/PEG mass ratios. The WCA on bare-AW was $66.3 \pm 0.8°$ because of the intrinsic hydrophilic property of stainless steel. When a cross-linked PEG network with hydrophilic characteristics was coated onto the surface, the WCA exhibited a statistically significant decrease to $34.8 \pm 0.8°$, which is favorable for the formation of a thin water layer and thus improves the adhesion-inhibiting performance. There was a slight increase in the WCA of CS/PEG-AW (0.05:1), CS/PEG-AW (0.1:1), and CS/PEG-AW (0.2:1), but a sharp increase ($55.3 \pm 0.6°$) was observed for CS/PEG-AW (0.4:1). This strong correlation between the WCA and the amount of CS may be due to its intrinsic hydrophobic property, which in turn leads to a slight increase in bacterial adhesion (Figure 3c). We further studied the surface potential of stainless-steel AWs with different chemical compositions. As shown in Figure 4c, there is no significant difference between bare AW and PEG-AW because of the uncharged nature of PEG molecules. With an increasing amount of CS, the surface potential decreased from approximately -32 to -21 mV, which indicated that the surface was becoming more positively charged.[28] It is well known that hydrophilic surfaces inhibit bacterial adhesion and that CS's positive charge contributes to suppressing bacterial colonization.[13] By balancing the effect of surface wettability and surface potential, the best antibacterial performance on CS/PEG-AW was obtained with a 0.1:1 CS/PEG mass ratio. Increasing the amount of CS any further might cause the surface to have an excessive positive charge, therefore facilitating the adsorption of bacteria because of their negatively charged cell membranes, and this would lead to a decrease in the hydrophilicity of the material, which is detrimental to the adhesion-inhibiting property. Therefore, we can conclude that combining the hydrophilic PEG network

with the positively charged CS results in CS/PEG primers that prevent the adhesion of bacteria and, at the same time, suppress bacterial colonization.

Longevity and safety are the main concerns for the clinical adoption of medical devices. To mimic the pathogenesis of medical device-associated infections, bacterial colonization of bare-AW, PEG-AW, and CS/PEG-AW in nutrient-rich conditions was investigated. In our experiments, bacteria were first seeded onto the samples and incubated for 1 d, allowing for bacterial settlement on the surfaces. The samples were then incubated for up to 7 d by dropping a fresh culture medium onto the surfaces every 24 h.[29] To investigate the efficiency of our designed primer in inhibiting bacterial growth, the bacteria on the treated samples were then vortexed and sonicated vigorously into a sterile saline solution.[30,31] The bacteria were then spread on Petri dishes using an easySpiral automatic plater (Figure 5a) to calculate the number of bacteria (N, cfu mL^{-1}) and antibacterial rate (eq 1) in each group.

$$\text{Antibacterial rate} = \frac{N(\text{control}) - N(\text{material})}{N(\text{control})} \times 100\%$$

(1)

where $N(\text{control})$ is the average colony count for the bare-AW samples and $N(\text{material})$ is the average colony count for the PEG-AW or CS/PEG-AW samples.

As shown in Figure 5b, the number of bacteria steadily increased on bare-AW as the incubation time was extended from 1 to 7 d. Although the initial bacterial adhesion on PEG-AW was significantly inhibited, bacterial colonization occurred after 7 d, suggesting that PEG-AW fails to suppress the growth of bacterial colonies. In contrast, CS/PEG-AW with optimal CS/PEG ratios of 0.1:1 always maintained very low bacterial adhesion regardless of the incubation time, resulting in a high antibacterial rate of approximately 90% (Figure 5c). It is worth noting that the antibacterial rate of CS/PEG-AW (0.1:1) was always the highest among all groups and showed a statistically significant difference when compared to that of PEG-AW, reaching up to 86.04, 91.59, 94.16, and 93.27% in 1, 3, 5, and 7 d respectively, which is consistent with the SEM and fluorescence images. These results demonstrate that AWs coated with CS/PEG primers have a persistent antibacterial activity against *S. mutans*.

Considering the application of the CS/PEG hydrogel in medical devices, the coating must maintain good stability. XPS analysis was used to examine the stability and applicability of the coating after immersion and tape tests (Figure S2d−f). The samples were immersed in a simulated body fluid after 7 d, and there was no obvious variation in their surface energy spectra, showing that the chemical stability of the CS/PEG copolymer and bioactivity of the coating are both satisfactory (Figure S2d,e). We further used a tape test to confirm the mechanical stability of the copolymer on the AWs. After 10 tape tests using 3M Scotch tape were performed, the surface energy spectrum of the CS/PEG-AW was almost unchanged (Figure S2d,f). The results showed that the CS/PEG coating was stable to physiological conditions for a long time and exhibited good bonding strength during mechanical changes. Moreover, to test the safety and biocompatibility of the samples due to their potential application in medical devices, a cholecystokinin octapeptide (CCK-8) cell viability assay was used to examine the cell proliferation characterization on surfaces functionalized with PEG or CS/PEG polymers after 1, 2, and 3 d of

incubation (Figure S4). In cell viability studies with the CCK-8 assay, lower values indicate increased cytotoxicity. The PEG and CS/PEG groups displayed cell viability similar to that of the bare group during all test periods, indicating that the copolymer group was as nontoxic as the other groups were. Moreover, the optical density values of the PEG and CS/PEG groups reached statistically significant increases when compared with those of the bare group after 3 d, which may indicate better biocompatibility.

3. CONCLUSIONS

In summary, by combining the hydrophilicity of the PEG network with the positively charged CS, we successfully synthesized a multifunctional CS/PEG hydrogel coating with good adhesion-inhibiting and colony-suppressing activity and biocompatibility, which has not been applied in implant medicine, especially dental areas. Introduction of a PEG-based cross-linked network onto the surface increased the hydrophilic properties of the material, thus enhancing its adhesion-inhibiting properties. Furthermore, the optimized mass ratio of CS/PEG (0.1:1) could provide polycationic structures to rupture the cell membrane without obviously decreasing the hydrophilicity, resulting in long-term bacterial colonization suppression. The present work provides new insights into the design and practice of multifunctional antibacterial coatings with promising potential in clinical applications.

4. EXPERIMENTAL DETAILS

4.1. Synthesis of PEG and CS/PEG-Modified Stainless-Steel Wires/Sheets and Silicon Wafers. The silanized surfaces, including stainless-steel wires/sheets and silicon wafers, were first prepared by successive ultrasonication in acetone, ethanol, and Milli-Q water at room temperature for 10, 10, and 15 min, respectively, to remove contamination from organic grease. The degreased silicon wafers were then heated in a boiling piranha solution (3:1 H_2SO_4/H_2O_2) for at least 1 h, while the stainless-steel wires/sheets were immersed in 0.1% NaOH aqueous solution for 30 s followed by immersion in 0.1% HNO_3 aqueous solution for 30 s. All substrates were thoroughly washed with Milli-Q grade water and then treated with oxygen plasma at 150 W for 15 min (Plasma Etch, Inc., USA). After these steps, silicon wafers and stainless-steel wires/sheets were incubated in a silanization solution for 24 h at room temperature. The silanization solution was prepared by diluting 0.5 mL of 3-(trimethoxysilyl) propyl methacrylate in 50 mL of methanol. The silanized substrates were rinsed with methanol and stored in a vacuum desiccator. The hydrogel-modified surfaces (to synthesize a thin layer of mPEG-DA on the silanized surfaces) were prepared by dissolving 0.125 g of mPEG-DA (M_w = 2000 Da) with or without different quantities (0.00625, 0.0125, 0.025, and 0.05 g) of CS in 5 mL of HAc (pH = 3). The solution was degassed by bubbling nitrogen into the solution for 30 min. Then, the silanized surfaces were submerged into the reaction mixture with ammonium persulfate as the initiator and maintained at 80 °C for 8 h. The substrates were rinsed thoroughly with HAc to remove the unbound polymer. Finally, these materials were thoroughly washed with deionized water three times and dried with a flow of nitrogen. The presence of CS/PEG coating on the stainless-steel wires/sheets was confirmed by XPS on a VG-ESCALAB 220i-XL system using 300 W Al Kα radiation as the excitation source and a base pressure of approximately 3×10^{-9} mbar. The binding energies were referenced to the C 1s line at 284.8 eV arising from adventitious carbon.

4.2. Thickness Measurement of the Polymeric Layer. CLSM images were taken to measure the thickness of the CS/PEG coating on an Olympus LEXT OLS4500 nano search microscope. The CS/PEG coating was fabricated on a smooth silicon wafer instead of the stainless-steel substrate prior to microscopy observation.

4.3. Fluorescence Microscopy. Fluorescence microscopy was used to investigate bacterial density and surface coverage after an *S. mutans* UA159 cell suspension was loaded onto the coated AWs and prestained with a LIVE/DEAD bacterial viability kit. The cells were imaged using a fluorescence microscope (Nikon, Ti-E) under Plan-Apochromat 40×/1.3 Oil DIC M27 objective lens. The excitation/ emission maxima for these dyes were approximately 480/500 nm for SYTO 9 stain and 490/635 nm for propidium iodide. In this experiment, 10 images were captured per group ($n = 10$).

4.4. Microscopic Morphology of PEG and CS/PEG Coatings. Because the surface roughness of stainless-steel wire will cause interferences, we investigated the microscopic morphology of the coatings using AFM. We chose silicon wafers to explore micromorphology of the bare, PEGylated, and CS/PEG coatings containing different CS/PEG mass ratios (0.05:1, 0.1:1, 0.2:1, and 0.4:1). The AFM images were obtained using a Dimension FastScan Bio AFM from Bruker with ScanAsyst in the air mode. The images were captured in the height sensor data type at a scan rate of 2.93 Hz with a size of 1 μm × 1 μm. The surface roughness of the materials is indicated by R_q.

4.5. Macroscopic Wettability of PEG and CS/PEG Coating. We evaluated the surface wettability of our PEG- and CS/PEG-coated stainless-steel sheets by measuring the WCA using a DataPhysics OCA20 contact angle measuring system (Filderstadt, Germany) at ambient temperature. Stainless-steel sheets with dimensions of 10 × 10 × 1.5 mm were chosen as the appropriate size for these experiments. A droplet of water (2 μL) was syringed out and dropped onto the underlying surface. Average CAs were obtained from three measurements performed at different positions on the same sample.

4.6. Electrical Characterization of PEG and CS/PEG Coating. Zeta potential measurements were performed using a Zetasizer Nano ZS instrument (Malvern Instruments, Worcestershire, UK). Stainless-steel sheets with dimensions of 3 × 5 × 0.25 mm were chosen as the appropriate size for these experiments. The zeta potential transfer standard (DTS1235) is a polystyrene latex standard in aqueous buffer at pH = 9 with a zeta potential of −42 mV ± 4.2 mV.

4.7. Longevity Antibacterial Test. To mimic the pathogenesis of device-associated infections, bacterial colonization of the contaminated surfaces in nutrient-rich conditions was then investigated. Prior to the in vitro antibacterial tests, *S. mutans* was grown overnight in brain heart infusion (BHI) broth at 37 °C. Overnight cultures of *S. mutans* were diluted to an optical density of 10^8 cells mL^{-1} in sterile BHI broth. After immersing the bare and PEG- and CS/PEG-coated AWs in the culture media for 1 d, they were washed with phosphate-buffered saline (PBS) to remove nonadherent bacteria, followed by dropping fresh BHI culture media onto the surfaces every 24 h. After 1, 3, 5, and 7 d, the samples were rinsed three times with sterile PBS to remove any nonadherent cells. The colonized native and treated samples were then transferred into 2 mL of sterile saline solution A and vortexed vigorously for 30 s. Next, the samples were transferred into 2 mL of sterile saline solution B and sonicated in a Branson 2200 sonicator for 3 min. The samples were then transferred once more into 2 mL of sterile saline solution C and vortexed vigorously for 30 s. Suspensions A, B, and C were pooled, diluted, and spread on Petri dishes using an easySpiral automatic plater. After overnight static incubation of the agar plates at 37 °C, the number of bacteria (N, cfu mL^{-1}) and the antibacterial rate were calculated, using bare-AW as a control group. The measurements were taken three times for each group ($n = 3$).

4.8. Statistical Analysis. The data are reported as the mean ± standard error for each sample. ImageJ (version 2.1.4.7) and Origin 8 software were used to analyze the images and plot the graphs, respectively. Each experiment was replicated at least three times. Statistical evaluation was performed using a one-way ANOVA ($p < 0.05$, $p < 0.01$) with the least significant difference test or Dunnett T3 test for pairwise comparisons versus the control group. All statistical analyses were performed using SPSS 22.0 software.

■ ASSOCIATED CONTENT

Ⓢ Supporting Information

The Supporting Information is available free of charge at https://pubs.acs.org/doi/10.1021/acsami.9b19873.

> Materials; bacterial cultivation; SEM imaging; bacteria LIVE/DEAD cell viability assay; cell culture; cell viability assays; tape test; immersion test; scheme of synthesis procedure of the CS/PEG hydrogel coating; full XPS spectra of bare-AW, silanized-AW, and CS/ PEG-AW and XPS spectra of CS/PEG coating after immersion test and tape test; SEM images of the surface morphology of bare-AW, PEG-AW, and CS/PEG-AW; cell proliferation characterization via CCK-8 assay on surfaces functionalized with PEG or CS/PEG polymers (PDF)

■ AUTHOR INFORMATION

Corresponding Authors

> **Yan Wei** − *Department of Geriatric Dentistry, Peking University School and Hospital of Stomatology, Beijing Laboratory of Biomedical Materials, Beijing 100081, P. R. China;* Email: kqweiyan@bjmu.edu.cn

> **Hongliang Liu** − *CAS Key Laboratory of Bio-inspired Materials and Interfacial Science, CAS Center for Excellence in Nanoscience, Technical Institute of Physics and Chemistry, Chinese Academy of Sciences, Beijing 100190, P. R. China;* ⓞ orcid.org/0000-0002-6781-3546; Email: liuhl@ mail.ipc.ac.cn

> **Bing Han** − *Department of Orthodontics, Peking University School and Hospital of Stomatology & National Engineering Laboratory for Digital and Material Technology of Stomatology & Beijing Key Laboratory of Digital Stomatology, Beijing 100081, P. R. China;* ⓞ orcid.org/0000-0003-4584-1092; Email: kqbinghan@bjmu.edu.cn

Authors

> **Liying Peng** − *Department of Orthodontics, Peking University School and Hospital of Stomatology & National Engineering Laboratory for Digital and Material Technology of Stomatology & Beijing Key Laboratory of Digital Stomatology, Beijing 100081, P. R. China*

> **Li Chang** − *CAS Key Laboratory of Bio-inspired Materials and Interfacial Science, CAS Center for Excellence in Nanoscience, Technical Institute of Physics and Chemistry, Chinese Academy of Sciences, Beijing 100190, P. R. China*

> **Mengting Si** − *Department of Geriatric Dentistry, Peking University School and Hospital of Stomatology, Beijing Laboratory of Biomedical Materials, Beijing 100081, P. R. China*

> **Jiuxiang Lin** − *Department of Orthodontics, Peking University School and Hospital of Stomatology & National Engineering Laboratory for Digital and Material Technology of Stomatology & Beijing Key Laboratory of Digital Stomatology, Beijing 100081, P. R. China*

> **Shutao Wang** − *CAS Key Laboratory of Bio-inspired Materials and Interfacial Science, CAS Center for Excellence in Nanoscience, Technical Institute of Physics and Chemistry, Chinese Academy of Sciences, Beijing 100190, P. R. China;* ⓞ orcid.org/0000-0002-2559-5181

> **Lei Jiang** − *CAS Key Laboratory of Bio-inspired Materials and Interfacial Science, CAS Center for Excellence in Nanoscience,*

■ REFERENCES

(1) Webber, M. J.; Appel, E. A.; Meijer, E. W.; Langer, R. Supramolecular Biomaterials. *Nat. Mater.* **2016**, *15*, 13−26.

(2) Tan, L.; Li, J.; Liu, X.; Cui, Z.; Yang, X.; Zhu, S.; Li, Z.; Yuan, X.; Zheng, Y.; Yeung, K.; Pan, H.; Wang, X.; Wu, S. Rapid Biofilm Eradication on Bone Implants Using Red Phosphorus and Near-Infrared Light. *Adv. Mater.* **2018**, *30*, 1801808.

(3) Liu, X.; Peng, L.; Meng, J.; Zhu, Z.; Han, B.; Wang, S. Protein-Mediated Anti-Adhesion Surface Against Oral Bacteria. *Nanoscale* **2018**, *10*, 2711−2714.

(4) Blair, J. M. A.; Webber, M. A.; Baylay, A. J.; Ogbolu, D. O.; Piddock, L. J. V. Molecular Mechanisms of Antibiotic Resistance. *Nat. Rev. Microbiol.* **2015**, *13*, 42−51.

(5) Campoccia, D.; Montanaro, L.; Arciola, C. R. A Review of the Biomaterials Technologies for Infection-Resistant Surfaces. *Biomaterials* **2013**, *34*, 8533−8554.

(6) Cloutier, M.; Mantovani, D.; Rosei, F. Antibacterial Coatings: Challenges, Perspectives, and Opportunities. *Trends Biotechnol.* **2015**, *33*, 637−652.

(7) Gref, R.; Minamitake, Y.; Peracchia, M.; Trubetskoy, V.; Torchilin, V.; Langer, R. Biodegradable Long-Circulating Polymeric Nanospheres. *Science* **1994**, *263*, 1600−1603.

(8) Prime, K.; Whitesides, G. Self-Assembled Organic Monolayers: Model Systems for Studying Adsorption of Proteins at Surfaces. *Science* **1991**, *252*, 1164−1167.

(9) Zhi, Z.; Su, Y.; Xi, Y.; Tian, L.; Xu, M.; Wang, Q.; Pandidan, S.; Li, P.; Huang, W. Dual-Functional Polyethylene Glycol-b-polyhexanide Surface Coating with in Vitro and in Vivo Antimicrobial and Antifouling Activities. *ACS Appl. Mater. Interfaces* **2019**, *9*, 10383.

(10) Peng, L.; Chang, L.; Liu, X.; Lin, J.; Liu, H.; Han, B.; Wang, S. Antibacterial Property of a Polyethylene Glycol-Grafted Dental Material. *ACS Appl. Mater. Interfaces* **2017**, *9*, 17688−17692.

(11) Zhang, J.; Shen, B.; Chen, L.; Chen, L.; Mo, J.; Feng, J. Antibacterial and Antifouling Hybrid Ionic-Covalent Hydrogels with Tunable Mechanical Properties. *ACS Appl. Mater. Interfaces* **2019**, *11*, 31594−31604.

(12) Shi, L.; Chen, J.; Teng, L.; Wang, L.; Zhu, G.; Liu, S.; Luo, Z.; Shi, X.; Wang, Y.; Ren, L. The Antibacterial Applications of Graphene and its Derivatives. *Small* **2016**, *12*, 4165−4184.

(13) Rabea, E. I.; Badawy, M. E.-T.; Stevens, C. V.; Smagghe, G.; Steurbaut, W. Chitosan as Antimicrobial Agent: Applications and Mode of Action. *Biomacromolecules* **2003**, *4*, 1457−1465.

(14) Vimala, K.; Mohan, Y. M.; Sivudu, K. S.; Varaprasad, K.; Ravindra, S.; Reddy, N. N.; Padma, Y.; Sreedhar, B.; MohanaRaju, K. Fabrication of Porous Chitosan Films Impregnated with Silver Nanoparticles: A Facile Approach for Superior Antibacterial Application. *Colloids Surf., B* **2010**, *76*, 248−258.

(15) Li, P.; Poon, Y. F.; Li, W.; Zhu, H.-Y.; Yeap, S. H.; Cao, Y.; Qi, X.; Zhou, C.; Lamrani, M.; Beuerman, R. W.; Kang, E.-T.; Mu, Y.; Li, C. M.; Chang, M. W.; Jan Leong, S. S.; Chan-Park, M. B. A Polycationic Antimicrobial and Biocompatible Hydrogel with Microbe Membrane Suctioning Ability. *Nat. Mater.* **2011**, *10*, 149−156.

(16) Dong, R.; Zhao, X.; Guo, B.; Ma, P. X. Self-Healing Conductive Injectable Hydrogels with Antibacterial Activity as Cell Delivery Carrier for Cardiac Cell Therapy. *ACS Appl. Mater. Interfaces* **2016**, *8*, 17138−17150.

(17) Bozuyuk, U.; Dogan, N. O.; Kizilel, S. Deep Insight into PEGylation of Bioadhesive Chitosan Nanoparticles: Sensitivity Study for the Key Parameters through Artificial Neural Network Model. *ACS Appl. Mater. Interfaces* **2018**, *10*, 33945−33955.

(18) Wang, B.; Liu, H.; Wang, Z.; Shi, S.; Nan, K.; Xu, Q.; Ye, Z.; Chen, H. A Self-Defensive Antibacterial Coating Acting through the Bacteria-Triggered Release of a Hydrophobic Antibiotic From Layer-By-Layer Films. *J. Mater. Chem. B* **2017**, *5*, 1498−1506.

(19) Zhao, X.; Wu, H.; Guo, B.; Dong, R.; Qiu, Y.; Ma, P. X. Antibacterial Anti-Oxidant Electroactive Injectable Hydrogel as Self-Healing Wound Dressing with Hemostasis and Adhesiveness for Cutaneous Wound Healing. *Biomaterials* **2017**, *122*, 34−47.

(20) Nitta, S.; Komatsu, A.; Ishii, T.; Ohnishi, M.; Inoue, A.; Iwamoto, H. Fabrication and Characterization of Water-dispersed Chitosan Nanofiber/Poly(ethylene glycol) Diacrylate/Calcium Phosphate-based Porous Composites. *Carbohydr. Polym.* **2017**, *174*, 1034−1040.

(21) Shutava, T. G.; Livanovich, K. S.; Sharamet, A. A. Layer-By-Layer Films of Polysaccharides Modified with Polyethylene Glycol and Dextran. *Colloids Surf., B* **2019**, *173*, 412−420.

(22) Yamashita, T.; Hayes, P. Analysis of XPS Spectra of Fe2+ and Fe3+ Ions in Oxide Materials. *Appl. Surf. Sci.* **2008**, *254*, 2441−2449.

(23) Zhang, F.; Kang, E. T.; Neoh, K. G.; Wang, P.; Tan, K. L. Surface Modification of Stainless Steel by Grafting of Poly(Ethylene Glycol) for Reduction in Protein Adsorption. *Biomaterials* **2001**, *22*, 1541−1548.

(24) Le, X. T.; Doan, N. D.; Dequivre, T.; Viel, P.; Palacin, S. Covalent Grafting of Chitosan onto Stainless Steel through Aryldiazonium Self-Adhesive Layers. *ACS Appl. Mater. Interfaces* **2014**, *6*, 9085−9092.

(25) Kingshott, P.; Thissen, H.; Griesser, H. J. Effects of Cloud-Point Grafting, Chain Length, and Density of PEG Layers on Competitive Adsorption of Ocular Proteins. *Biomaterials* **2002**, *23*, 2043−2056.

(26) Santiago-Bautista, L.; Hdz-García, H. M.; Muñoz-Arroyo, R.; Alvarez-Vera, M.; García-García, A.; Mtz-Enriquez, A. I.; Hernández-García, F. A.; Acevedo-Dávila, J. L. Growth of a graphenic-Co Composite Coating on Type-304 Stainless Steel. *Vacuum* **2019**, *163*, 324−327.

(27) Loesche, W. J. Role of Streptococcus mutans in Human Dental Decay. *Microbiol. Rev.* **1986**, *50*, 353−380.

(28) Zhang, C.; Liu, W.; Cao, C.; Zhang, F.; Tang, Q.; Ma, S.; Zhao, J.; Hu, L.; Shen, Y.; Chen, L. Modulating Surface Potential by Controlling the Beta Phase Content in Poly(vinylidene Fluoridetrifluoroethylene) Membranes Enhances Bone Regeneration. *Adv. Healthcare Mater.* **2018**, *7*, 1701466.

(29) Yan, S.; Song, L.; Luan, S.; Xin, Z.; Du, S.; Shi, H.; Yuan, S.; Yang, Y.; Yin, J. A Hierarchical Polymer Brush Coating with Dual-Function Antibacterial Capability. *Colloids Surf., B* **2017**, *150*, 250−260.

(30) Ignatova, M.; Voccia, S.; Gilbert, B.; Markova, N.; Cossement, D.; Gouttebaron, R.; Jérôme, R.; Jérôme, C. Combination of Electrografting and Atom-Transfer Radical Polymerization for Making the Stainless Steel Surface Antibacterial and Protein Antiadhesive. *Langmuir* **2006**, *22*, 255−262.

(31) Cavoue, T.; Bounou Abassi, H.; Vayssade, M.; Nguyen Van Nhien, A.; Kang, I.-K.; Kwon, G.-W.; Pourceau, G.; Dubot, P.; Abbad

Andaloussi, S.; Versace, D.-L. Imidazolium-Based Titanium Substrates Against Bacterial Colonization. *Biomater. Sci.* **2017**, *5*, 561−569.